Journal of Materials Chemistry A

COMMUNICATION

View Article Online
View Journal | View Issue

Cite this: J. Mater. Chem. A, 2015, 3, 7215

Received 17th January 2015
Accepted 5th March 2015

DOI: 10.1039/c5ta00379b

www.rsc.org/MaterialsA

Facile preparation of an ultrathin sulfur-wrapped polyaniline nanofiber composite with a core–shell structure as a high performance cathode material for lithium–sulfur batteries†

Hong Gao,[ab] Qi Lu,[a] Nianjiang Liu,[a] Xianhong Wang*[a] and Fosong Wang[a]

An ultrathin sulfur layer (10 nm) wrapped polyaniline (PANI) nanofiber composite (S–PANI) with a core–shell structure was prepared *via* facile heterogeneous nucleation of sulfur on a water-dispersed PANI nanofiber, which displayed an initial discharge capacity of 977 mA h g^{-1} and a capacity retention of 88.3% after 100 cycles at 1 C.

The lithium–sulfur (Li–S) battery shows a great possibility as a promising successor for the next generation high-energy-density battery. One reason is that it has a theoretical specific energy of *ca.* 2600 W h kg^{-1}, which is more than 5 times that of a conventional lithium ion battery, as calculated from the electrochemical reaction $16Li + S_8 \rightarrow 8Li_2S$, and another advantage lies in that sulfur is inexpensive, abundant on the earth, and well suitable for large-scale practical applications.[1] Nevertheless, the practical application of Li–S batteries has not yet been achieved because of some challenges like low practical capacity and poor cycle performance, especially at a high charge–discharge rate, mainly due to the insulating feature of sulfur, significant structure and volumetric change during the cycling process, and the "shuttle" phenomenon caused by the high solubility of intermediate reduction products Li_2S_x $(2 < x \leq 8)$ in organic electrolytes.[2–4]

In recent years, much effort has been made to fabricate high performance Li–S batteries. The electronic conductivity and structural stability of the cathode were enhanced by combining sulfur with conducting matrices, commonly carbon materials like microporous carbon,[5] mesoporous carbon,[6,7] engineered hierarchical porous carbon,[8] hollow carbon spheres,[9] carbon nanotubes,[10] carbon nanofibers[11] and grapheme.[12–14] Recently, Chen and co-workers designed a layered porous carbon–sulfur composite consisting of a graphene layer with thin layers of porous carbon uniformly covering both surfaces, which showed a very high initial discharge capacity of 885 mA h g^{-1} at 0.5 C and a capacity retention of 70% after running 100 cycles.[15] Nazar and coworkers confined sulfur in 4–5 nm mesopores in the shell and inner lining of the carbon nanospheres; a specific capacity of over 875 mA h g^{-1} was achieved at 1 C with a fade rate of 0.1% per cycle.[16] The sulfur in these materials was in the nano-scale, which not only improved its utilization but also increased the contact area with conducting matrices. And just like these, confining sulfur in the pores of various carbon materials has been a usual strategy to prevent the loss of soluble polysulfides. However, the physical encapsulation method is not as perfect as expected. Further research by Cui's group showed that the insoluble Li_2S/Li_2S_2 would detach from the carbon surface during discharge due to the low binding energy between the nonpolar carbon and polar Li_2S/Li_2S_2 clusters, resulting in the loss of electrical contact and capacity decay.[17] Therefore, to effectively hold sulfur within the conducting materials, attention should be focused on designing more reasonable structures or developing an alternative matrix to carbon.

Inspired by the above reports, we tried to search a positively charged conducting matrix replacing carbon materials to combine with sulfur in the nano-scale. Compared with the single physical adsorption of carbon materials, the electrostatic interaction of a positively charged conducting matrix to negatively charged S_x^{2-} $(2 < x \leq 8)$ could be stronger during the charge–discharge process. Conducting polymers may meet the need by positively charging the backbones through acid doping. In fact, previous reports proved that they surely have the abilities to absorb and hold sulfur.[18–25] Here, we chose polyaniline (PANI) nanofibers with requisite positively charged backbones as the matrix material. Compared with the S–PANI composite previously reported, the PANI nanofibers used here were thinner (with an average diameter of 70 nm) and water-dispersed which ensured that an organic solvent was non-essential and all preparation processes could be carried out in water. Beyond that, no thermal treatment was applied from the

[a]Key Laboratory of Polymer Eco-materials, Changchun Institute of Applied Chemistry, Chinese Academy of Sciences, Changchun 130022, People's Republic of China. E-mail: xhwang@ciac.jl.cn; Fax: +86 431 85689095; Tel: +86 431 85262250

[b]University of Chinese Academy of Sciences, Beijing 100039, People's Republic of China

† Electronic supplementary information (ESI) available: Experimental details and additional data. See DOI: 10.1039/c5ta00379b

beginning to the end, so the conducting matrix maintained its original structure and conductivity. To ensure the efficient ion transmission and electron transport at different discharge rates, sulfur was deposited on the outer surface of the PANI nanofiber. The thickness of this sulfur layer was determined to be 10 nm, nearly equalling the maximum thickness of a typical electric double layer on the surface of the electrode.[26] That could, for one thing, maximize the utilization of electrostatic interactions, and for another, increase the sulfur content in this composite as high as possible. The sulfur content in this designed composite could be calculated by the following equation:

$$S\% = w_s/(w_s + w_{PANI}) \quad (1)$$

Eqn (1) could be further derived as eqn (2) (for more detailed discussion see the ESI†):

$$t_S = r\left\{\left[\left(\frac{S\%}{1-S\%} + \frac{\gamma\rho_S}{\rho_{PANI}}\right)\frac{\rho_{PANI}}{\gamma\rho_S}\right]^{1/2} - 1\right\} \quad (2)$$

where S% is the sulfur content in the composite, w_s is the mass of sulfur, w_{PANI} is the mass of PANI, γ is the correction factor (approximately equals to 1.0), ρ_S is the sulfur density (1.96 g cm^{-3}), ρ_{PANI} is the PANI density (0.75 g cm^{-3}), r is the PANI radius (35 nm), and t_S is the thickness of the sulfur layer (10 nm). It was easily concluded that the sulfur content in this composite was no less than 60%, a relatively high value for the sulfur electrode material. By adjusting the experimental conditions, finally we successfully prepared this ultrathin sulfur-wrapped PANI nanofiber for the first time.

Referring to the former work of our group, the water-dispersed conducting PANI nanofibers with a diameter of about 70 nm were synthesized in a large quantity and used as a template to prepare the sulfur-wrapped PANI composite by the heterogeneous nucleation reaction.[27,28] The zeta potential of PANI was about +45.17 mV, so thiosulfate ions could be adsorbed around the positively charged PANI nanofibers easily during the nucleation reaction. Next, elemental sulfur nucleated on the dispersed PANI substrates after the dropwise addition of sulphuric acid solution into the mixture. All the reactions were carried out in water at an ambient atmosphere without heating, the facile synthesis process made it suitable for large-scale preparation. The PANI nanofibers used here showed a high BET specific surface area of 77.14 $m^2\ g^{-1}$ and a total pore volume of 0.24 $cm^3\ g^{-1}$, which were very important for effective sulfur deposition. After the deposition process, the sulfur could fill the void of PANI nanofibers, since the BET surface area and the pore volume of S–PANI dropped to 24.33 $m^2\ g^{-1}$and 0.12 $cm^3\ g^{-1}$, respectively (Fig. 1a).

The sulfur loading in the S–PANI composite was determined by thermogravimetric analysis (TGA). As shown in Fig. 1b, the elemental sulfur started to lose its weight at 120 °C and lost its all weight at 300 °C, while PANI exhibited a little weight loss (12.18%) within this range of temperature, mainly due to the loss of moisture and decomposition of PANI itself. As for S–PANI composites, considering the low content of PANI in this composite, the weight loss of inner PANI could be ignored during sulfur evaporation, and it was easy to conclude that the sulfur loading was about 65%.

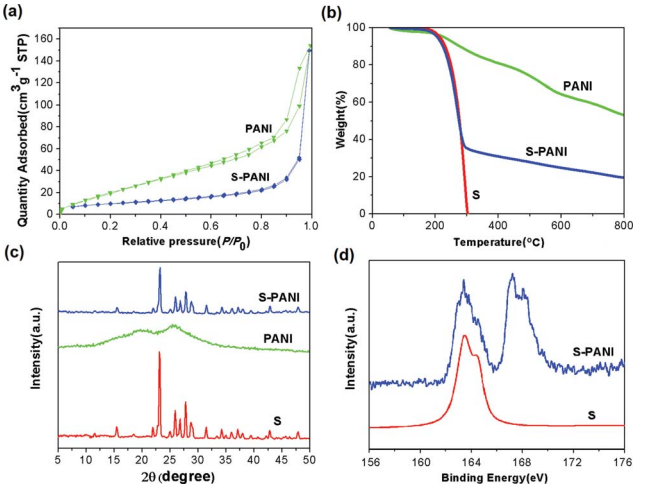

Fig. 1 (a) Nitrogen adsorption/desorption isotherms of PANI and S–PANI; (b) TGA curves of S, PANI, and S–PANI; (c) XRD patterns of S, PANI, and S–PANI; (d) XPS spectra of S 2p for S and S–PANI.

Fig. 1c shows the X-ray diffraction (XRD) patterns of elemental sulfur, PANI nanofiber and S–PANI composite, respectively. Two prominent peaks at $2\theta = 23$ and 28° corresponding to an F_{ddd} orthorhombic structure can be observed in the XRD pattern of elemental sulfur, while the XRD pattern of the PANI nanofiber shows two broad, low-intensity peaks centered at $2\theta = 19.1$ and 25.4°, which could be assigned to the periodicity parallel and perpendicular to the PANI chains, respectively. The diffraction peaks of elemental sulfur are visible in the XRD pattern of the S–PANI composite, though the intensities become distinctly lower, which indicates that the sulfur formed by heterogeneous nucleation retained its original crystal structure.

X-ray photoelectron spectroscopy (XPS) was used to study sulfur wrapping on PANI. Fig. 1d shows S 2p spectra of S–PANI and sulfur produced by mixing sodium thiosulfate with sulfuric acid. Two types of S atoms in S–PANI were observed at binding energies of 167.15 and 163.35 eV. The one at 167.15 eV came from the dopant SO_4^{2-}, which replaced the initial dopant phosphate ester during the acid titration process, and the other at 163.35 eV matched well with the characteristic peak of sulfur implying that sulfur had deposited on the polyaniline nanofiber successfully.

The morphology characterization of the S–PANI composite was carefully investigated by scanning electron microscopy (SEM) and transmission electron microscopy (TEM). Fig. 2a shows the SEM image of the S–PANI composite. It displayed a neat wire-like shape. The SEM elemental mapping images (Fig. 2b) displayed matching spatial distributions of C, N and S, indicating the uniform distribution of sulfur in the S–PANI composite. EDX microanalysis (lower right image in Fig. 2b) exhibited a strong sulfur signal, which was higher than carbon. The existence of oxygen was from the dopant SO_4^{2-}. TEM was

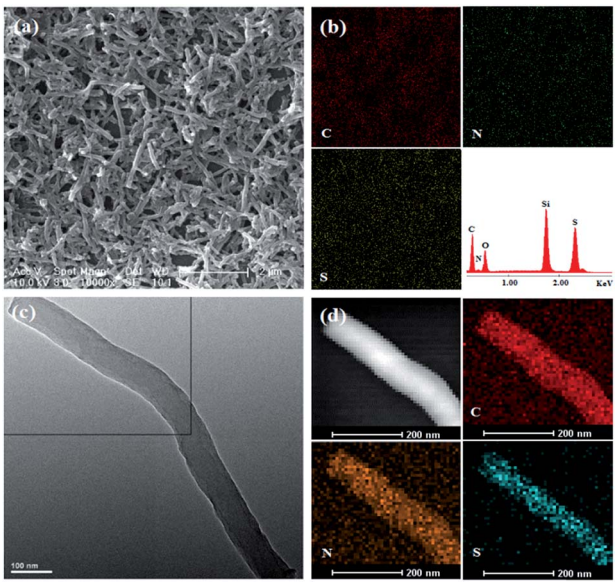

Fig. 2 Morphology of the S–PANI composite: (a) SEM image; (b) SEM elemental maps of carbon (upper left), nitrogen (upper right), sulfur (lower left), and the EDX pattern (lower right); (c) TEM image; (d) dark-field TEM (upper left), and EDX elemental mappings of carbon (upper right), nitrogen (lower left) and sulfur (lower right).

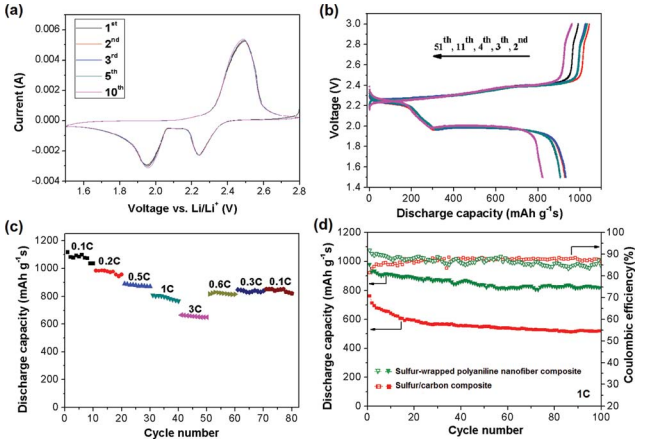

Fig. 3 (a) Cyclic voltammograms of the S–PANI composite; (b) discharge–charge voltage profiles of the S–PANI composite at 1 C; (c) rate performance of the S–PANI composite at various cycling rates from 0.1 to 3 C with respect to the cycle number; (d) cycle stability of the S–PANI composite and the S–C composite at 1 C.

used to further study the core–shell structure and track the elemental distribution of carbon, nitrogen and sulfur in the S–PANI composite. The S–PANI composite was fiber-like with a diameter of about 90 nm, and the thickness of sulfur wrapped on the PANI nanofiber was just *ca.* 10 nm. However, the boundary between sulfur and PANI was very clear even under such thin sulfur coverage. As shown in Fig. 2d, sulfur can maintain uniform distribution on a single PANI nanofiber.

The above morphology characterization confirmed that the ultrathin sulfur-wrapped polyaniline nanofiber composite was successfully synthesized. This well-designed structure was beneficial for electrochemical performance. Inner conductive PANI nanofibers formed an effective and stable electron transport system, like carbon materials. During charge–discharge progress, the positively charged backbone could hold negatively charged S_x^{2-} ($2 < x \leq 8$) by the electrostatic interaction, which ensured its cycle stability, while the outer extremely thin layer of sulfur made the diffusion of ions between cathode and electrolyte easier and faster, showing the potential of high utilization of active materials and good electrochemical performance at a high discharge rate. The electrochemical performances of S–PANI composite cathodes were examined in CR2016-type coin cells, which were fabricated by sandwiching a porous polypropylene separator (Celgard 2500) between the S–PANI electrode and Li foil and the electrolyte was 1.0 M lithium bis(trifluoromethane) sulfonamide (LiTFSI) in a mixed solvent of 1,3-dioxolane (DOL) and 1,2-dimethoxyethane (DME) (1 : 1, v/v).

Fig. 3a shows the cyclic voltammogram (CV) curves of the S–PANI nano-composite. During the first reduction process, two main reduction peaks appeared at around 2.24 V and 1.95 V, characteristic of the two-step reduction of elemental sulfur, the first step was the transformation from cyclo-octasulfur (S_8) to long-chain soluble lithium polysulfides (Li_2S_x, $4 \leq x < 8$), while the second step corresponded to the decomposition of polysulfides to form insoluble short-chain lithium sulfides (Li_2S_2 and/or Li_2S). In the subsequent anodic scan, the oxidation peak was found at around 2.49 V, which corresponded to the conversion of Li_2S to high-order soluble polysulfides.[25] The cyclic voltammograms showed no obvious change in the following scans up to 10 cycles, indicating excellent reversibility and cycling stability of the S–PANI composite.

Fig. 3b shows the galvanostatic charge–discharge profiles of the S–PANI electrode at 1 C during different cycles. There are two apparent discharge plateaus and one charge plateau on each curve, which matches well with the CV measurements. The decrease of specific capacity was insignificant with the increasing cycle number, *e.g.*, the fourth cycle and the eleventh cycle were even superposition.

Fig. 3c shows the rate capacity performance of the S–PANI composite electrode. After an initial discharge capacity of 1116 mA h g^{-1} at 0.1 C, the capacity was found to stabilize around 1080 mA h g^{-1}, and it was 980 mA h g^{-1} at 0.2 C. Further cycling at 0.5, 1 and 3 C, it still showed high reversible capacities of 890, 808 and 655 mA h g^{-1}, respectively. When the current density was switched from 3 to 0.6 C, the specific capacity was largely recovered at the 51st cycle, indicating good reversible stability of this cathode material.

This composite cathode showed superior electrochemical performance producing a high initial discharge capacity of 977 mA h g^{-1} at 1 C. Since the second cycle, the specific capacity stabilized at high capacities of approximately 900 mA h g^{-1} and 88.3% of the initial capacity was retained after 100 cycles (Fig. 3d). As a reference, the sulfur/carbon composite was prepared by ball-milling and 180 °C thermal treatment, an initial discharge capacity of 762 mA h g^{-1} was obtained, and it dropped to 520 mA h g^{-1} after 100 cycles. This comparison clearly showed that the core–shell structure of the sulfur-

wrapped PANI composite could offer more advantages to improve the electrochemical performance of the Li–S battery than the traditional sulfur/carbon material.

In summary, an ultrathin sulfur-wrapped PANI nanocomposite was well-designed and successfully prepared by a very simple and soft route. This novel S–PANI composite exhibited a high initial discharge capacity of 977 mA h g^{-1} and a capacity retention of 88.3% after 100 cycles at 1 C, which represents the best comprehensive performance among the PANI composites used in Li–S batteries so far. The high specific capacity and good cycle stability at the high rate demonstrated the rationality of this special three-dimensional structure. The conducting PANI nanofiber with a positively charged backbone not only acted like stable carbon materials transmitting electrons but also could hold negatively charged S_x^{2-} $(2 < x \leq 8)$ around it during the charge–discharge process. In addition, the ultrathin sulfur layer on the outer surface made ion transmission faster and more convenient, meanwhile, the utilization of the active material was largely improved compared with the traditional S–C material.

Acknowledgements

The authors thank financial support from the Natural Science Foundation of China (Grant no. 51321062 and 51303168).

Notes and references

1 D. Bresser, S. Passerini and B. Scrosati, *Chem. Commun.*, 2013, **49**, 10545–10562.
2 A. Manthiram, Y. Fu and Y. S. Su, *Acc. Chem. Res.*, 2013, **46**, 1125–1134.
3 M. K. Song, E. J. Cairns and Y. Zhang, *Nanoscale*, 2013, **5**, 2186–2204.
4 L. Chen and L. L. Shaw, *J. Power Sources*, 2014, **267**, 770–783.
5 S. Xin, L. Gu, N. H. Zhao, Y. X. Yin, L. J. Zhou, Y. G. Guo and L. J. Wan, *J. Am. Chem. Soc.*, 2012, **134**, 18510–18513.
6 X. Ji, K. T. Lee and L. F. Nazar, *Nat. Mater.*, 2009, **8**, 500–506.
7 J. Schuster, G. He, B. Mandlmeier, T. Yim, K. T. Lee, T. Bein and L. F. Nazar, *Angew. Chem., Int. Ed.*, 2012, **51**, 3591–3595.
8 B. Ding, C. Yuan, L. Shen, G. Xu, P. Nie and X. Zhang, *Chem.–Eur. J.*, 2013, **19**, 1013–1019.
9 N. Jayaprakash, J. Shen, S. S. Moganty, A. Corona and L. A. Archer, *Angew. Chem., Int. Ed.*, 2011, **50**, 5904–5908.
10 J. Guo, Y. Xu and C. Wang, *Nano Lett.*, 2011, **11**, 4288–4294.
11 G. Zheng, Y. Yang, J. J. Cha, S. S. Hong and Y. Cui, *Nano Lett.*, 2011, **11**, 4462–4467.
12 K. Xi, P. R. Kidambi, R. Chen, C. Gao, X. Peng, C. Ducati, S. Hofmann and R. V. Kumar, *Nanoscale*, 2014, **6**, 5746–5753.
13 J. Zhang, Z. Dong, X. Wang, X. Zhao, J. Tu, Q. Su and G. Du, *J. Power Sources*, 2014, **270**, 1–8.
14 H. Kim, H. D. Lim, J. Kim and K. Kang, *J. Mater. Chem. A*, 2014, **2**, 33–47.
15 X. Yang, L. Zhang, F. Zhang, Y. Huang and Y. Chen, *ACS Nano*, 2014, **8**, 5208–5215.
16 G. He, S. Evers, X. Liang, M. Cuisinier, A. Garsuch and L. F. Nazar, *ACS Nano*, 2013, **7**, 10920–10930.
17 G. Zheng, Q. Zhang, J. J. Cha, Y. Yang, W. Li, Z. W. Seh and Y. Cui, *Nano Lett.*, 2013, **13**, 1265–1270.
18 Y. Zhang, Z. Bakenov, Y. Zhao, A. Konarov, T. N. L. Doan, M. Malik, T. Paron and P. Chen, *J. Power Sources*, 2012, **208**, 1–8.
19 Z. Dong, J. Zhang, X. Zhao, J. Tu, Q. Su and G. Du, *RSC Adv.*, 2013, **3**, 24914–24917.
20 Y. Liu, J. Zhang, X. Liu, J. Guo, L. Pan, H. Wang, Q. Su and G. Du, *Mater. Lett.*, 2014, **133**, 193–196.
21 F. Wu, J. Chen, R. Chen, S. Wu, L. Li, S. Chen and T. Zhao, *J. Phys. Chem. C*, 2011, **115**, 6057–6063.
22 M. Wang, W. Wang, A. Wang, K. Yuan, L. Miao, X. Zhang, Y. Huang, Z. Yu and J. Qiu, *Chem. Commun.*, 2013, **49**, 10263–10265.
23 Y. Fu and A. Manthiram, *J. Phys. Chem. C*, 2012, **116**, 8910–8915.
24 W. Zhou, Y. Yu, H. Chen, F. J. DiSalvo and H. D. Abruña, *J. Am. Chem. Soc.*, 2013, **135**, 16736–16743.
25 L. Xiao, Y. Cao, J. Xiao, B. Schwenzer, M. H. Engelhard, L. V. Saraf, Z. Nie, G. J. Exarhos and J. Liu, *Adv. Mater.*, 2012, **24**, 1176–1181.
26 H. P. V. Leeuwen and W. Köster, *Physicochemical Kinetics and Transport at Biointerfaces*, Wiley, 2004.
27 H. Zhang, Q. Zhao, S. Zhou, N. Liu, X. Wang, J. Li and F. Wang, *J. Power Sources*, 2011, **196**, 10484–10489.
28 S. Zhou, H. Zhang, Q. Zhao, X. Wang, J. Li and F. Wang, *Carbon*, 2013, **52**, 440–450.

